Surface Reconstruction from Scattered Point via RBF Interpolation on GPU

Salvatore Cuomo*, Ardelio Galletti†, Giulio Giunta†, Alfredo Starace†
*Department of Mathematics and Applications "R. Caccioppoli" University of Naples Federico II
c/o Universitario M.S. Angelo 80126 Naples Italy
email:salvatore.cuomo@unina.it
†Department of Applied Science. University of Naples "Parthenope".
Centro Direzionale, Isola C4 80143 Naples Italy
emails:{ardelio.galletti,giulio.giunta}@uniparthenope.it, alfredo.starace@gmail.com

arXiv:1305.5179v1 [cs.DC] 22 May 2013

***Abstract*—In this paper we describe a parallel implicit method based on radial basis functions (RBF) for surface reconstruction. The applicability of RBF methods is hindered by its computational demand, that requires the solution of linear systems of size equal to the number of data points. Our reconstruction implementation relies on parallel scientific libraries and is supported for massively multi-core architectures, namely Graphic Processor Units (GPUs). The performance of the proposed method in terms of accuracy of the reconstruction and computing time shows that the RBF interpolant can be very effective for such problem.**

I. Introduction

Many applications in engineering and science need to build accurate digital models of real-world objects defined in terms of *point cloud data*, *i.e.* a set of scattered points in 3D. Typical examples include the digitalization of manufactured parts for quality control, statues and artifacts in archeology and arts [10], human bodies for movies or video games, organs and anatomical parts for medical diagnostic [4] and elevation models for simulations and modeling [14]. Using modern 3D scanners, it is possible to acquire point clouds containing millions of points sampled from an object. The process of building a geometric model from such point clouds is usually referred to as *surface reconstruction*.

There are several approaches to reconstruct surfaces from 3D scattered datasets. Generally, the methods of surface reconstruction fall into two categories [15]: Delaunay-based methods and volumetric and implicit based methods. Delaunay triangulation is usually utilized to find the possible neighbors for each point in all directions from all samples. Implicit surface modeling instead is most popular for describing complex shapes and complex editing operations. Among them, level set methods [23], moving least square methods [9], variational implicit surfaces [20] and adaptively sampled distance field [8] are recent developments in this field. In this paper we focus on the implicit surface method based on radial basis functions (RBFs). In the 1980's, Franke [7] used radial basis functions to interpolate scattered point cloud firstly and proved the accuracy and stability of the interpolation based on RBFs. Using this technique, an implicit surface is constructed by calculating the weights of a set of radial basis functions whose linear combination interpolates the given data points.

The RBF applicability is hindered by its computational demand, since these methods require the solution of a linear system of size equal to the number of data points and current 3D data scanners allow acquisition of tens of millions points of an object surface.

High Performance Computing (HPC) is a natural solution to provide the computational power required in such situations. In this paper we propose a method designed for a massively multi-core architecture, namely Graphics Processing Units (GPUs) [17]. Recently, GPUs have been effectively used to accelerate the performance of applications in several scientific areas such as computational fluid dynamics, molecular dynamics, climate modeling [6]. For our knowledge, the most efficient parallel algorithm for RBF interpolation is "PetRBF" [21]. PetRBF is a parallel algorithm for RBF interpolation that exhibits $\mathcal{O}(N)$ complexity, requires $\mathcal{O}(N)$ storage, and scales excellently up to a thousand processes. Our main contribute is a deep re-engineering of PetRBF which constitutes a generalization for scattered 3D data and an extension for GPU acceleration on heterogeneous clusters. We also focus on the suitable choice of the algorithm parameters and present an optimal strategy for synthetic, real or incomplete datasets.

In section II we deal mathematical Preliminaries, in section III we describe the related works and the implementation strategies. The section IV we report the numerical experiments and finally we draw conclusions in section V.

II. Preliminaries

In this section we recall the reconstruction based on implicit surface method and define the related RBF interpolation problem.

A. Implicit Surface Reconstruction

Given a point cloud

$$\mathcal{X} := \{(x_i, y_i, z_i) \in \mathbb{R}^3, i = 1, \ldots, N\}$$

coming from an unknown surface $\mathcal{M}$, *i.e.* $\mathcal{X} \subset \mathcal{M}$, the goal is to find another surface $\mathcal{M}^*$ which is a reconstruction of $\mathcal{M}$. In the implicit surface approach $\mathcal{M}$ is defined as the surface of all points $(x, y, z) \in \mathbb{R}^3$ that satisfy the implicit equation

$$f(x, y, z) = 0 \tag{1}$$

for an unknown function f. A way to approximate f is to impose the interpolation conditions (1) on the point cloud $\mathcal{X}$. However, the use of those interpolation conditions only leads to the trivial solution given by the identically zero function, whose zero surface is $\mathbb{R}^3$. Therefore, the key for finding an approximation of the function f is to use additional significant interpolation conditions, *i.e.* on correspondence of off-surface points (where $f \neq 0$). This involves a nontrivial interpolant $\mathcal{P}_f$, whose zero surface contains a meaningful surface $\mathcal{M}^*$. This approach leads to a surface reconstruction method which consists of three main steps:

1) generation of off-surface points;
2) interpolant model identification on the extended dataset;
3) computation of the interpolation zero iso-surface.

1) Generation of off-surface points:
A common practice, as suggested in [19], is to use the set of surface normals $\mathbf{n}_i = (n_i^x, n_i^y, n_i^z)$ to the surface $\mathcal{M}$ at points $\mathbf{x}_i = (x_i, y_i, z_i)$. If these normals are not explicitly known, there are techniques and tools[1] that to allow to estimate them. Given the oriented surface normals ($\mathbf{n}_i$ and $-\mathbf{n}_i$), we generate the extra off-surface points by marching a small distance δ along the normals. So, we obtain for each cloud data point $\mathbf{x}_i = (x_i, y_i, z_i)$ two additional off-surface points. The first lies "outside" the surface $\mathcal{M}$ and is given by

$$\begin{aligned}(x_{N+i}, y_{N+i}, z_{N+i}) &= \mathbf{x}_i + \delta \mathbf{n}_i = \\ &= (x_i + \delta n_i^x, y_i + \delta n_i^y, z_i + \delta n_i^z);\end{aligned}$$

the other point lies "inside" and is given by

$$\begin{aligned}(x_{2N+i}, y_{2N+i}, z_{2N+i}) &= \mathbf{x}_i - \delta \mathbf{n}_i = \\ &= (x_i - \delta n_i^x, y_i - \delta n_i^y, z_i - \delta n_i^z).\end{aligned}$$

The union of the sets $\mathcal{X}_\delta^+ = \{\mathbf{x}_{N+1}, \ldots, \mathbf{x}_{2N}\}$, $\mathcal{X}_\delta^- = \{\mathbf{x}_{2N+1}, \ldots, \mathbf{x}_{3N}\}$ and $\mathcal{X}$ gives the overall set of points on which the interpolation conditions are assigned (see Fig. 1). The set $\mathcal{X}_\delta^+$ implicitly defines a surface $\mathcal{M}_\delta^+$ which passes

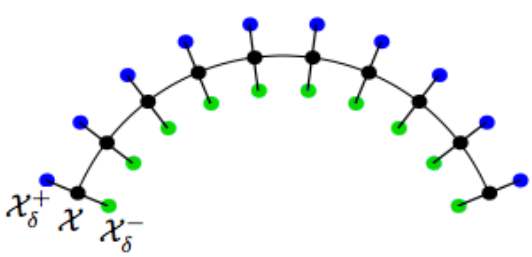

Fig. 1. Extended interpolation data set. In black points from $\mathcal{X}$, in blue points from $\mathcal{X}_\delta^+$ and in green points from $\mathcal{X}_\delta^-$

through its points. Analogously $\mathcal{X}_\delta^-$ defines the surface $\mathcal{M}_\delta^-$. Those two surfaces can be considered respectively external and internal to $\mathcal{M}$. The value of δ represents a small step size whose specific magnitude may be rather critical for a good surface reconstruction [3]. In particular, if δ is chosen too large, this results in self intersecting $\mathcal{M}_\delta^+$ or $\mathcal{M}_\delta^-$ auxiliary surfaces. In our implementation we fix δ to 1% of the bounding box of the data as suggested in [22].

2) Interpolant model identification on extended dataset:
This step consists in determining a function $\mathcal{P}_f$ whose zero contour interpolates the given point cloud data $\mathcal{X}$ and whose iso-surface $\mathcal{P}_f = 1$ and $\mathcal{P}_f = -1$ interpolate $\mathcal{X}_\delta^+$ and $\mathcal{X}_\delta^-$, respectively, *i.e.*

$$\mathcal{P}_f(x_i) = \begin{cases} 0 & i = 1, \ldots, N \\ 1 & i = N+1, \ldots, 2N \\ -1 & i = 2N+1, \ldots, 3N \end{cases}$$

The values of ± 1 for the auxiliary data are assigned in an arbitrary way. Such choice does not affect the quality of the results. In this discussion we are interested to the iso-surface zeros of $\mathcal{P}_f$.

3) Computation of the interpolation zero iso-surface:
In order to evaluate the $\mathcal{P}_f$ zero iso-surface and visualize it, we use a simple strategy which consists on evaluating the interpolant $\mathcal{P}_f$ on a dense grid of a bounding box. This approach leads to some undesired artifacts, since in the bounding box there are points that do not belong to $\mathcal{M}^*$. A possible way to overcome this drawback and display only $\mathcal{M}^*$ consists in evaluating the interpolant only in a small *surrounding* volume of the surface $\mathcal{M}$ to reconstruct. This set is denoted as $\mathcal{M}_{ext}^\varepsilon = \{\mathbf{x} \in \mathbb{R}^3 : \ d(\mathbf{x}, \mathcal{M}) \leq \varepsilon\}$, where $d(\mathbf{x}, \mathcal{M}) = \inf_{\mathbf{y} \in \mathcal{M}} \|\mathbf{y} - \mathbf{x}\|$. For a small enough value of ε it holds

$$\mathcal{M}^* \approx \mathcal{M}_{ext}^\varepsilon \cap \mathcal{S}_0.$$

where $\mathcal{S}_0$ is the zero iso-surface of $\mathcal{P}_f$.

B. RBF interpolation

Given a set of N distinct points $(x_j, \ y_j)$, $j = 1, \ldots, N$, where $x_j \in \mathbb{R}^s$ and $y_j \in \mathbb{R}$, the scattered data interpolation problem is to find an interpolant function $\mathcal{P}_f$ such that:

$$\mathcal{P}_f(x_j) = y_j, \ j = 1, \ldots, N. \tag{2}$$

In the univariate setting, the interpolant $\mathcal{P}_f$ is usually chosen in suitable spaces of functions. A common approach assumes that the function $\mathcal{P}_f$ is a linear combination of certain basis function B_j, *i.e.*

$$\mathcal{P}_f(x) = \sum_{j=1}^{N} c_j B_j(x). \tag{3}$$

In the multivariate setting ($x_j \in \mathbb{R}^s, \ s > 1$), however, the problem is much more complex. As stated by the *Mairhuber-Curtis* theorem [5], [11], in order to have a well-posed multivariate scattered data interpolation problem it is not possible to fix in advance the basis $\{B_1, \ldots, B_N\}$. Instead the basis must depend on the data location.

In order to obtain data dependent approximation space, as suggested by the Mairhuber-Curtis theorem, the RBF interpolation uses radial functions:

$$B_j \equiv \Phi_j = \varphi(\|x - x_j\|).$$

[1]package ply.tar.gz provided by Greg Turk, available at http://www.cc.gatech.edu/projects/large_models/ply.html

The points x_j to which the basic function φ is shifted are usually referred as *centers*. While there may be circumstances that suggest to choose these centers different from the data sites one generally picks the centers to coincide with the data sites.

The interpolation problem consists of two subproblems: finding the interpolant $\mathcal{P}_f$ and evaluating it on an assigned set of points. The coefficients c_j in (3) are obtained by imposing the interpolation conditions (2)

$$\mathcal{P}_f(x_i) = \sum_{j=1}^{N} c_j \varphi(\|x_i - x_j\|) = y_i, \; i = 1, \ldots, N.$$

This leads to solve a linear system of equations (4).

Given a set of M points $\xi = \{\xi_1, \xi_2, \ldots, \xi_M\}$ the evaluation of the interpolant $\mathcal{P}_f$ on ξ can be computed with a matrix vector product (5)

The RBF interpolant determination consists to solve a linear system of equations $Ax = b$. In order to have a well-posed problem the matrix A must be non-singular. Unfortunately no one has yet succeeded in characterizing the class of all basic function φ that generates a non-singular matrix for arbitrary set $\mathcal{X} = \{x_1, \ldots, x_N\}$ of distinct data sites. The situation is however much better with *positive definite matrices*. An important property of positive definite matrices is that all their eigenvalues are positive, and therefore a positive definite matrix is non-singular. Popular radial basis function Φ, that give rise to positive definite interpolation matrices, are summarized in Table II-B, we focused our work (as [21]) on the Gaussian function taking advantage of its property as described in §3.

III. Parallel Surface Reconstruction

A brief description of the overall surface reconstruction algorithm is listed below:

Algorithm 1 Surface Reconstruction

Requirements:
point cloud $\mathcal{X}$, surface normals $\mathbf{n}_i$, evaluation grid ξ

1: compute extended data set: $\mathcal{X}_{ext} = \mathcal{X} \bigcup \mathcal{X}_\delta^+ \bigcup \mathcal{X}_\delta^-$ by using $\mathbf{n}_i$;
2: find the interpolant $\mathcal{P}_f$ on $\mathcal{X}_{ext}$;
3: evaluate $\mathcal{P}_f$ on ξ;
4: render the surface;

The steps 1 and 2 have been already discussed in §2.1; the step 3 requires a matrix vector multiplication as described in §2.2 and the final step can be simply accomplished using the MATLAB software with the command `isosurface` or other specific tool for the rendering. The most computational expensive step is the second one, which requires the solution of a system of $3N$ linear equation, where N is the initial point cloud size, as described in §2.2. In the following section we describe the approach used to handle this problem.

A. Adopted solution

Handling problems with large numbers of data points, as in our case for surface reconstruction from clouds of millions of points, the large amount of memory usage can become a problem. As the problem size grows, parallelization on distributed memory architectures becomes necessary. We adopt the idea behind Domain Decomposition Methods (DDM) that is to divide the considered domain into a number of subdomains and then try to solve the original problem as a series of subproblems that interact through the interfaces. Let consider the domain Ω containing the point cloud; the adopted domain decomposition method divides the domain Ω in overlapping sub-domains Ω_i. The corresponding empty intersection portions of subdomains are denoted with $\tilde{\Omega}_i$, as shown in the example in Fig. 2. The solution of the linear

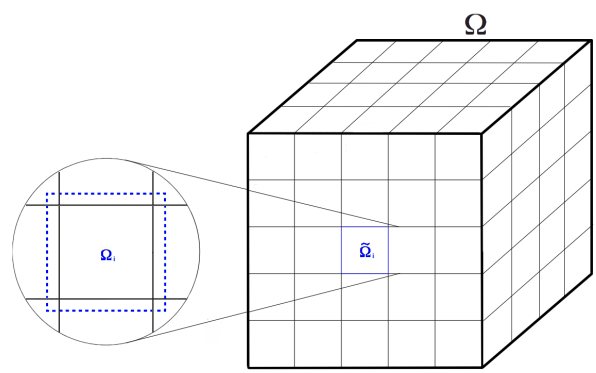

Fig. 2. Illustration of the Domain Decompostion Method.

system $Ax = b$ on the whole domain can be obtained by sequentially solving, in the individual overlapping subdomains Ω_i, the linear sub-system $A_i x_{\Omega_i} = b_{\Omega_i}$, where A_i, x_{Ω_i} and b_{Ω_i} are the sub-elements corresponding to domain Ω_i for A, x, and b respectively. When each subdomain is solved individually and the solution of the entire domain is updated simultaneously at the end of each iteration step, the method is called *additive* Schwarz method. Moreover, when the values x outside of the subdomain $\tilde{\Omega}_i$ are discarded after the calculation of each subdomain Ω_i, it is called *restricted additive* Schwarz method (RASM). The RASM is known to converge faster than the additive Schwarz method and requires less communication in parallel calculations. Furthermore solving smaller systems of equations has the same effect as a preconditioner, and then it can be used in combination with any iterative method like the Krylov subspace methods. In this work we use the Generalized Minimum Residual (GMRES).

Using basis functions with negligible global effects, the matrix A can be considered to have a finite bandwidth. In this case, the calculation of the matrix-vector multiplication, which is the predominant operation of the iterative solver, can be done somewhat locally. Using the Gaussian function as the basic function the matrix A has the following elements:

$$A_{ij} = \frac{1}{\sqrt{2\pi}\sigma} \exp\left(\frac{-\|\mathbf{x}_i - \mathbf{x}_j\|^2}{2\sigma^2}\right). \tag{6}$$

$$\underbrace{\begin{bmatrix} \varphi(\|x_1-x_1\|) & \varphi(\|x_1-x_2\|) & \cdots & \varphi(\|x_1-x_N\|) \\ \varphi(\|x_2-x_1\|) & \varphi(\|x_2-x_2\|) & \cdots & \varphi(\|x_2-x_N\|) \\ \vdots & \vdots & \ddots & \vdots \\ \varphi(\|x_N-x_1\|) & \varphi(\|x_N-x_2\|) & \cdots & \varphi(\|x_N-x_N\|) \end{bmatrix}}_{A} \cdot \underbrace{\begin{bmatrix} c_1 \\ c_2 \\ \vdots \\ c_N \end{bmatrix}}_{x} = \underbrace{\begin{bmatrix} y_1 \\ y_2 \\ \vdots \\ y_N \end{bmatrix}}_{b} \tag{4}$$

$$\begin{bmatrix} \mathcal{P}_f(\xi_1) \\ \mathcal{P}_f(\xi_2) \\ \vdots \\ \mathcal{P}_f(\xi_M) \end{bmatrix} = \begin{bmatrix} \varphi(\|\xi_1-x_1\|) & \varphi(\|\xi_1-x_2\|) & \cdots & \varphi(\|\xi_1-x_N\|) \\ \varphi(\|\xi_2-x_1\|) & \varphi(\|\xi_2-x_2\|) & \cdots & \varphi(\|\xi_2-x_N\|) \\ \vdots & \vdots & \ddots & \vdots \\ \varphi(\|\xi_M-x_1\|) & \varphi(\|\xi_M-x_2\|) & \cdots & \varphi(\|\xi_M-x_N\|) \end{bmatrix} \cdot \begin{bmatrix} c_1 \\ c_2 \\ \vdots \\ c_N \end{bmatrix} \tag{5}$$

TABLE I
EXAMPLES OF RADIAL BASIS FUNCTIONS.

RBF	Φ	
Poisson radial function	$\frac{J_{s/2-1(\|x-x_j\|)}}{\|x-x_j\|^{s/2-1}}$	$s \geq 2$
Inverse Multiquadric	$(1+\|x-x_j\|^2)^{-\beta}$	$\beta > \frac{s}{2}$
Matèrn function	$\frac{K_\alpha(\|x-x_j\|)\|x-x_j\|^\alpha}{2^{\beta-1}\Gamma(\beta)}$	$\alpha = \beta - \frac{s}{2} > 0$
Whittaker function	$\int_0^{+\infty}(1-\|x-x_j\|)_+^{k-1} t^\alpha e^{-\beta t} dt$	$k = 2, 3, \ldots, \quad \alpha = 0, 1, \ldots$
Gaussian function	$\frac{1}{\sqrt{2\pi}\sigma} e^{\frac{-\|x-x_j\|^2}{2\sigma^2}}$	$\sigma > 0$

In this way, since the Gaussian function decays rapidly, the elements of matrix A corresponding to the interaction of distant points can be neglected. This sparsity of A depends on the relative size of the calculation domain compared to the standard deviation, σ, of the Gaussian function. If σ is kept constant while the size of the calculation domain is increased along with N, the calculation load will scale as $\mathcal{O}(N)$. The communication required to perform Ax_i is also limited to a constant number of elements in the vicinity. Therefore, the RASM becomes an extremely parallel algorithm with minimum communication for the surface reconstruction problems that have a domain size of hundreds (or even thousands) of sigmas.

B. Implementation details

The algorithm implementation has been realized using the Portable, Extensible Toolkit for Scientific Computation (PETSc) [1]. PETSc is a scalable solver library developed at Argonne National Laboratory. All vectors and matrices can be distributed by PETSc and each process stores only a local portion. This transparent management of PETSc allows users to develop scalable parallel code (almost) as serial code. In particular this is done by using the `Vec` PETSc object for vectors x and b. To handle the overlapping and non-overlapping subdomain the index sets (`IS`) were used. The PETSc `IS` object is a global index that is used to define the elements in each subdomain and is distributed among the processes in the same way as the vectors. The interpolation matrix has entries which depends only from the vector $\mathbf{x}$ and the Gaussian (eq. 6). For this reason it is possible to use the `MatShell` object which allow to make operations on the matrix without actually storing the matrix. All calculation of inner products, norms, and scalar multiplications are done by calling PETSc routines and the linear system solution is finally calculated with `KSPSolve`.

C. GPU implementation

GPU support has recently been added to PETSc to exploit the performance of GPUs, these chips are highly optimized for graphics-related operations. We use the CUDA framework that greatly simplifies the programming model for GPUs. The GPU implementation of PETSc also uses some of those libraries. Instead of writing completely new CUDA code, PETSc uses the open source libraries CUSP [13] e Thrust [18]. This allows transparent utilization of the GPU without changing the existing source code of PETSc.

A new GPU specific Vector and Matrix classes called `VecCUSP` and `MatCUSP` has been implemented in PETSc. The classes use CUBLAS, CUSP, as well as Thrust library routines to perform matrix and vector operations on the GPU. The idea behind these libraries is to use already developed, fine tuned CUDA implementations with PETSc instead of developing new ones. The PETSc implementation acts as an interface between PETSc data structures and the external CUDA libraries Thrust and CUSP.

Using the `VecSetType()` and `MatSetType()` PETSc routines, users can switch to the GPU version of the application simply using the command line parameters `-vec_type cusp` and `-mat_type aijcusp`. Cusp natively supports several sparse matrix formats:

- Coordinate list (COO)
- Compressed Sparse Row (CSR)

- Diagonal (DIA)
- ELLPACK (ELL)
- Hybrid (HYB)

This feature is still in development in PETSc, however it can be used specifying `--download-txpetscgpu --with-txpetscgpu=1` in the configuration and compilation phase of PETSc. After that it is possible for the application to switch between the sparse matrix formats with the command line option `-mat_cusp_storage_format <format>`.

A simple GPU implementation can be obtained by passing to the `MatShell` a pointer to a function that call a CUDA kernel that execute the operations on the Matrix. A better idea is to use the GPU version of PETSc objects whenever possible, in order to accelerate all the available operation, and not only those on the matrix. To this end there is the need of building the matrices object. The Matrix for the interpolant determination (step 2) can be easily constructed using the algorithm reported in Algorithm 2. For the interpolant evaluation (step 3) instead the only required operation is the matrix vector multiplication. For this reason the construction of the matrix and the following matrix-vector multiplication done directly by PETSc using CUSP is less efficient than a custom matrix-vector multiplication CUDA kernel (Algorithm 3) that consider the well known structure of the matrix (eq. 6) without the need of building the Matrix.

Algorithm 2 Interpolation matrix construction Pseudo-code algorithm

1: **for each** subdomain Ω_i **do**
2: **for each** point x_i in the subdomain Ω_i **do**
3: **for each** point x_j in the truncation area of Ω_i **do**
4: Set $A_{ij} = \frac{1}{\sqrt{2\pi}\sigma} \exp\left(\frac{-\|x_i - x_j\|^2}{2\sigma^2}\right)$
5: **end for**
6: **end for**
7: **end for**

Algorithm 3 CUDA code of RBF evaluation algorithm

```
1: __shared__ float sharedXi[BLOCK_SIZE];
2: __shared__ float sharedGi[BLOCK_SIZE];
3: int bx = blockIdx.x;
4: int tx = threadIdx.x;
5: int i = blockIdx.x * BLOCK_SIZE +
   threadIdx.x;
6: float pf = 0;
7: float coeff = 0.5f/(sigma*sigma);
8: for (unsigned int m = 0; m <
   (col-1)/BLOCK_SIZE+1; m++) {
9: sharedXi[tx] = Xi[m*BLOCK_SIZE + tx];
10: __syncthreads();
11: for (unsigned int k = 0; k <
   BLOCK_SIZE; k++) {
12: dx = Xj[i]-sharedXi[k];
13: pf += sharedGi[k]*exp(-(dx*dx)*coeff;}}
14: Pf[i] = pf/M_PI*coef;
```

IV. Experimental results

In this section we present some results of our method for surface reconstruction. The results presented here were computed using a system equipped with an Intel Core i7-940 CPU (2,93 GHz, 8M Cache). The middleware framework is OS Linux kernel 2.6.32-28 and PETSc developer version 3.3.

Tests has been conducted to investigate the impact of the parameter σ on the quality of the reconstruction. As showed in §3.2 our method is highly efficient for small value of σ compared to the domain size. However, besides efficiency, the quality of the result also depends strongly on the value of σ. This is because the accuracy of the interpolation model depends strongly on the ratio between the density of the point cloud and σ.

In [21] experiments are carried out only on equally-spaced lattice point distributions. In this particular case they used as a measure for the density the spacing h between the points, discovering that a good choice for σ, in term of performance and accuracy, is the one that satisfy the ratio $h/\sigma \approx 1$.

For widely scattered data, as in the case of points cloud for surface reconstruction, there are more appropriate density measure available. The first is the so-called *separation distance* defined as

$$q_{\mathcal{X}} = \frac{1}{2} \min_{i \neq j} \|x_i - x_j\|_2. \tag{7}$$

As shown in Fig. 3, $q_{\mathcal{X}}$ geometrically represents the radius of the largest (hyper)sphere that can be drawn around each point in such a way that no (hyper)sphere intersects the others, which is why it is also sometimes called *packing radius*. Another measure, usually used in approximation theory, is the so-called *fill distance*:

$$h_{\mathcal{X},\Omega} = \sup_{x \in \Omega} \min_{x_j \in \mathcal{X}} \|x - x_j\|_2. \tag{8}$$

It indicates how well the set $\mathcal{X}$ fill the domain Ω. A geometric interpretation of the fill distance is given by the radius of the biggest empty (hyper)sphere that can be placed among the data locations in Ω (see Fig. 3), for this reason it sometimes is also used as synonym the term *covering radius*. Hence for scattered data, using (7) and (8), the heuristic "optimal" ratio $h/\sigma \approx 1$ assumes the following expressions:

$$\sigma \approx 2q_{\mathcal{X}} \tag{9}$$

and

$$\sigma \approx h_{\mathcal{X},\Omega}\sqrt{2}. \tag{10}$$

A. Tests on synthetic dataset

We first conduct some experiment on a synthetic dataset. We choose as surface a sphere, whose geometry is well know, and on which it is possible to calculate (7) and (8). In order to perform a consistent test with real dataset, we use a widely scattered point cloud reported in Fig. 4.

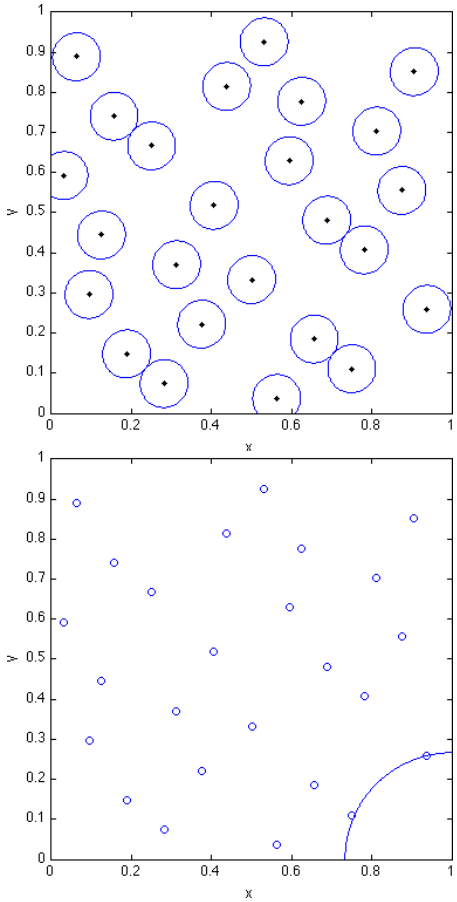

Fig. 3. Geometric interpretation of separation distance (on the left) and fill distance (on the right) for 25 Halton points on the domain $\Omega = [0,1]^2$ ($q_{\mathcal{X}} \approx 0.0597$ and $h_{\mathcal{X},\Omega} \approx 0.2667$).

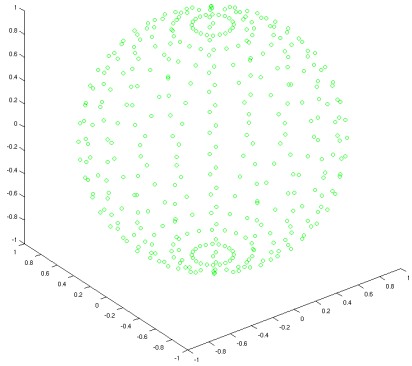

Fig. 4. 382 point cloud from the unit radius sphere centered in the origin.

As shown in Fig. 5 (top left) a value of σ too small leads to a surface that actually interpolates the given point cloud but whose reconstruction quality is total unsatisfactory. Neither using (9), as in [21], is enough for scattered data (see Fig. 5, top right). Increasing the value of σ (Fig. 5, bottom left) the quality of the reconstruction improves up to the desired one (Fig. 5, bottom right) using (10). It is interesting to note that for intermediate values of σ, though the quality is not globally satisfactory, it is locally sufficient for areas where the points

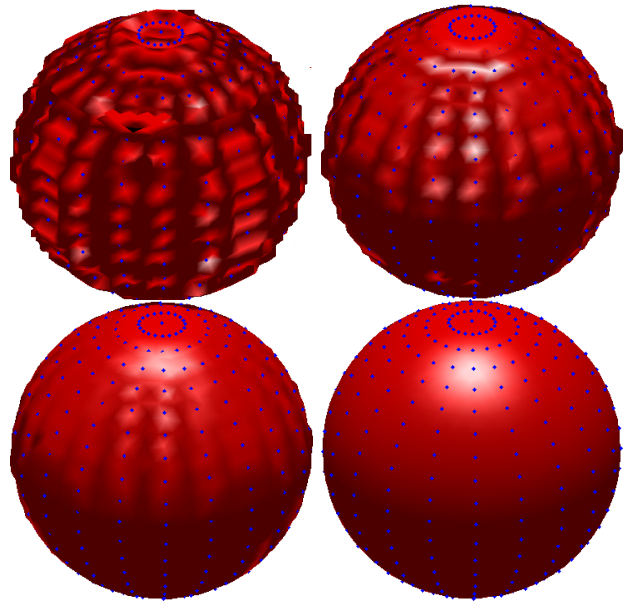

Fig. 5. Reconstructed sphere for different values of σ. (from left to right $\sigma = 0.025$, $\sigma = 2q_{\mathcal{X}} = 0.048$, $\sigma = 0.065$, $\sigma = h_{\mathcal{X},\mathcal{M}}\sqrt{2} = 0.157$)

are at a distance $d \approx \sigma$.

1) Tests on incomplete data:
We test the sensitivity of the algorithm to the lack of information using incomplete dataset. We first use a dataset composed of 50% randomly chosen points of the previous dataset. As shown in Fig. 6 the point cloud is changed, then also the "optimal" value for σ changes and becomes

$$\sigma = h_{\mathcal{X},\mathcal{M}}\sqrt{2} = 0.328.$$

We remark that the previous value of $\sigma = 0.157$ leads to a reconstructed surface which is not the desired sphere (Fig. 6, top). Instead, by using the optimal value $\sigma = 0.328$, corresponding to the actual fill distance for the new dataset, we successfully reconstruct the sphere once again (Fig. 6, bottom).

For a second test we use a point cloud coming from the upper semi-sphere:

$$\mathcal{M}^+ = \{(x,y,z) \in \mathbb{R}^3 : \; x^2 + y^2 + z^2 = 1, z \geq 0\}.$$

Using the value $\sigma = 0.157$ which equals to $h_{\mathcal{X},\mathcal{M}^+}\sqrt{2}$, as shown in Fig.7 (top), we reconstruct with success the $\mathcal{M}^+$ surface from which we took the data set. Instead, if we assume that the point cloud came from the whole sphere $\mathcal{M}$, the value of the fill distance changes to $h_{\mathcal{X},\mathcal{M}} = \sqrt{2}$. Using this value we get an optimal value of $\sigma = h_{\mathcal{X},\mathcal{M}}\sqrt{2} = 2$, which leads to the reconstruction of the whole sphere as shown in Fig. 7 (bottom).

B. Tests on real dataset

Finally we test our optimal choice of σ on real dataset using the Stanford Bunny model. The dataset we used is composed of $N = 8171$ points which leads to an the extended dataset of $N_{ext} = 3N = 24513$ points. In order to select

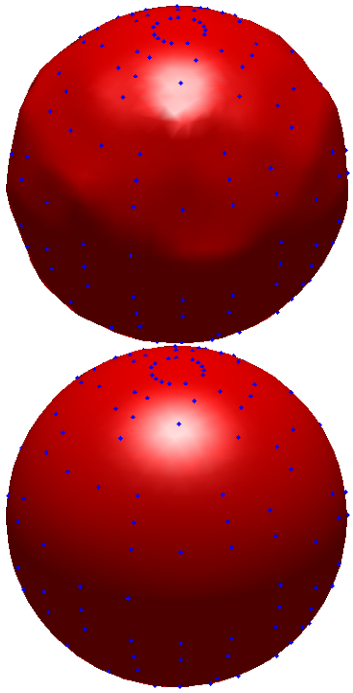

Fig. 6. Reconstructed sphere from incomplete data. (on the left $\sigma = 0.157$ and on the right $\sigma = h_{\mathcal{X},\mathcal{M}}\sqrt{2} = 0.328$)

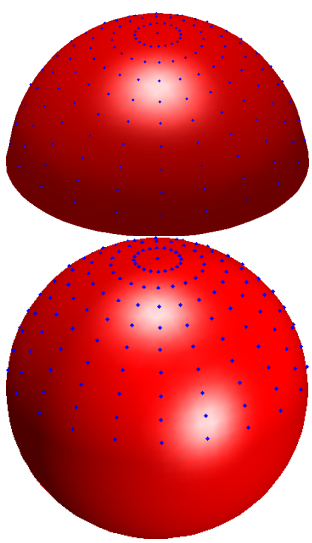

Fig. 7. Reconstructed surface from upper semi-sphere data. (on the left $\sigma = h_{\mathcal{X},\mathcal{M}^+}\sqrt{2} = 0.157$ and on the right $\sigma = h_{\mathcal{X},\mathcal{M}}\sqrt{2} = 2$)

the optimal value of σ one need to calculate the value of the fill distance. On real datasets, where the geometry of the surface in unknown or at least really complex, this task is a real challenge. Recalling that the fill distance measures the data density in the membership domain we introduce a new measure defined as

$$h_{max} = \max_j \min_{i \neq j} \|x_i - x_j\|_2.$$

This represents the bigger distance among the distances calculated between each point and its closer point. For a dataset without multiple *connected components*, the fill distance can be approximated by

$$h_{\mathcal{X},\mathcal{M}} \approx h_{max}\sqrt{2}. \tag{11}$$

As in synthetic data set, a value of σ too small results in a low quality reconstructed surface (Fig. 8(top left)), intermediate values leads to reconstructions with locally good reconstruction for areas with high density points (Fig. 8, top right) and a using (11) a choice of $\sigma \approx h_{\mathcal{X},\mathcal{M}}$ is the optimal one (Fig. 8, bottom).

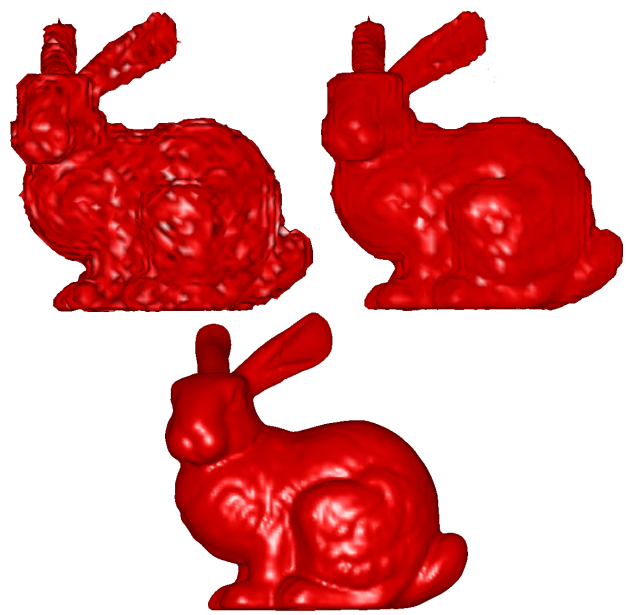

Fig. 8. Reconstructed bunny for different values of σ. (from left to right $\sigma = 0.0007$, $\sigma = 0.0012$ and $\sigma = h_{max} \approx h_{\mathcal{X},\mathcal{M}}\sqrt{2} = 0.0033$)

C. Tests on performance

In this section, we will discuss the performance of our GPU implementation on a single node compared to the CPU implementation. CPU times refers to the execution on one core of i7-940 CPU and the GPU times refers to execution on a nVIDIA Fermi C1060 GPU with 4Gb of RAM. The middleware software consists of PETSc developer version 3.3 compiled with GPU support, CUDA release 4.2, CUSP version 0.3.0 and Thrust version 1.5.2.

For our tests we used a synthetic point cloud dataset with an increasing number N of points. Increasing the number of points of the cloud corresponds to increasing the density of the domain. For this reason, since we want to emphasize the benefits of the GPU, we used a constant value of $\sigma = 0.157$. Otherwise with a value of σ scaled with the density the problem would scale as $\mathcal{O}(N)$ making less noticeable the contribution of the GPU.

In Tab. II we report the execution time on a single CPU and GPU and the resulting speed up for the determination of the interpolant (step 2 of the reconstruction algorithm) varying the size N of the data. To make a fair comparison we fixed the number of iteration of the GMRES to 50. Results in Tab. II

shows that, even if the RASM preconditioner is not available in CUSP, exploiting the GPU the execution time can be greatly decreased.

TABLE II
SPEED UP WITH GPU FOR INTERPOLANT DETERMINATION.

N	CPU	GPU	Speed up
1323	0,67551	0,1404	4,81
4686	34,567	5,6472	6,12
15625	451,75	71,57	6,31
24036	5398,4	815,09	6,63

In Tab. III are reported the execution time on CPU and GPU with the resulting speed up for the interpolant evaluation (step 3 of the surface reconstruction algorithm) varying the size N of the point cloud and the size M of the evaluation grid. As expected these execution time are substantially lower than those for the previous problem but in this case the GPU is fully exploited obtaining greater speed ups.

TABLE III
SPEED UP WITH GPU FOR EVALUATION OF INTERPOLANT.

$M \backslash N$		1323	4686	15625	24036
15625	CPU	0,11571	0,20605	0,78172	0,97539
	GPU	0,012831	0,033589	0,12167	0,13699
	Speed up	**9,01**	**6,13**	**6,42**	**7,12**
125000	CPU	0,60406	1,5657	5,9558	7,433
	GPU	0,029907	0,09974	0,32034	0,43697
	Speed up	**20,19**	**15,69**	**18,59**	**17,01**
421875	CPU	1,9098	5,2612	19,946	25,037
	GPU	0,084603	0,2892467	0,89695	1,1272
	Speed up	**22,57**	**18,18**	**22,23**	**22,211**
1000000	CPU	4,4389	12,505	47,594	59,501
	GPU	0,18456	0,60741	2,0629	2,4968
	Speed up	**24,05**	**20,58**	**23,07**	**23,83**
1953125	CPU	8,8515	24,431	92,589	116,39
	GPU	0,35668	1,0662	3,9195	4,8035
	Speed up	**24,81**	**22,91**	**23,62**	**24,23**
3375000	CPU	15,018	42,166	160,17	199,45
	GPU	0,59846	1,7525	6,4671	7,9468
	Speed up	**25,09**	**24,06**	**24,76**	**25,09**

V. CONCLUSION

We have implemented a parallel implicit method based on radial basis functions for surface reconstruction. This implementation relies on parallel scientific libraries and is supported for the GPU device. Since the reconstruction quality and the performances are strongly related to the gaussian RBF parameter σ, we propose an optimal and heuristic estimate based on some density measures of the point cloud. Finally, the obtained speed-up and running time confirm that the RBF interpolant can be a very effective algorithm for such problem.

REFERENCES

[1] Satish Balay, William Gropp, Lois Curfman McInnes, and Barry F Smith. Petsc, the Portable, Extensible Toolkit for scientific computation. *Argonne National Laboratory*, 2:17, 1998.

[2] R.K. Beatson, WA Light, and S. Billings. Fast solution of the radial basis function interpolation equations: Domain decomposition methods. *SIAM Journal on Scientific Computing*, 22(5):1717–1740, 2001.

[3] Jonathan C Carr, Richard K Beatson, Jon B Cherrie, Tim J Mitchell, W Richard Fright, Bruce C McCallum, and Tim R Evans. Reconstruction and representation of 3d objects with radial basis functions. In *Proceedings of the 28th annual conference on Computer graphics and interactive techniques*, pages 67–76. ACM, 2001.

[4] Jonathan C. Carr, W. Richard Fright, and Richard K Beatson. Surface interpolation with radial basis functions for medical imaging. *Medical Imaging, IEEE Transactions on*, 16(1):96–107, 1997.

[5] P.C. Curtis. n-parameter families and best approximation. *Pacific Journal of Mathematics*, 9(4):1013–1027, 1959.

[6] Cuomo, S. De Michele, P. Farina, R.Piccialli, F. A Smart GPU Implementation of an Elliptic Kernel for an Ocean Global Circulation Model, *Applied Mathematical Sciences*, Vol. 7, no. 61, 3007 - 3021 (2013).

[7] R. Franke. Scattered data interpolation: Tests of some methods. *Math. Comput.*, 38(157):181–200, 1982.

[8] Sarah F Frisken, Ronald N Perry, Alyn P Rockwood, and Thouis R Jones. Adaptively sampled distance fields: a general representation of shape for computer graphics. In *Proceedings of the 27th annual conference on Computer graphics and interactive techniques*, pages 249–254. ACM Press/Addison-Wesley Publishing Co., 2000.

[9] Jan Klein and Gabriel Zachmann. Point cloud surfaces using geometric proximity graphs. *Computers & Graphics*, 28(6):839–850, 2004.

[10] Marc Levoy, Kari Pulli, Brian Curless, Szymon Rusinkiewicz, David Koller, Lucas Pereira, Matt Ginzton, Sean Anderson, James Davis, Jeremy Ginsberg, Jonathan Shade, and Duane Fulk. The digital michelangelo project: 3d scanning of large statues. In *Proceedings of the 27th annual conference on Computer graphics and interactive techniques*, SIGGRAPH '00, pages 131–144. ACM Press/Addison-Wesley Publishing Co., 2000.

[11] J.C. Mairhuber. On haar's theorem concerning chebychev approximation problems having unique solutions. *Proceedings of the American Mathematical Society*, pages 609–615, 1956.

[12] WR Madych and SA Nelson. Multivariate interpolation and conditionally positive definite functions. ii. *Mathematics of Computation*, 54(189):211–230, 1990.

[13] Nathan Bell and Michael Garland. Cusp: Generic parallel algorithms for sparse matrix and graph computations, 2012. Version 0.3.0.

[14] Joachim Pouderoux, Jean-Christophe Gonzato, Ireneusz Tobor, and Pascal Guitton. Adaptive hierarchical rbf interpolation for creating smooth digital elevation models. In *Proceedings of the 12th annual ACM international workshop on Geographic information systems*, GIS '04, pages 232–240. ACM, 2004.

[15] Oliver Schall and Marie Samozino. Surface from scattered points. In *a Brief Survey of Recent Developments. 1st International Workshop on Semantic Virtual Environments, Page (s)*, pages 138–147, 2005.

[16] B. Smith, P. Bjorstad, and W. Gropp. *Domain decomposition: parallel multilevel methods for elliptic partial differential equations*. Cambridge University Press, 2004.

[17] J Süßmuth, Q Meyer, and G Greiner. Surface reconstruction based on hierarchical floating radial basis functions. In *Computer Graphics Forum*, volume 29, pages 1854–1864. Wiley Online Library, 2010.

[18] Jared Hoberock and Nathan Bell. Thrust: A parallel template library, 2010. Version 1.5.2.

[19] Greg Turk, Huong Quynh Dinh, James F O'Brien, and Gary Yngve. Implicit surfaces that interpolate. In *Shape Modeling and Applications, SMI 2001 International Conference on.*, pages 62–71. IEEE, 2001.

[20] Greg Turk and James F O'brien. Variational implicit surfaces. 1999.

[21] Rio Yokota, L.A. Barba, and Matthew G. Knepley. Petrbf a parallel o(n) algorithm for radial basis function interpolation with gaussians. *Computer Methods in Applied Mechanics and Engineering*, 199(25):1793 – 1804, 2010.

[22] H. Wendland. *Scattered data approximation*, volume 2. Cambridge University Press Cambridge, 2005.

[23] Hong-Kai Zhao, Stanley Osher, and Ronald Fedkiw. Fast surface reconstruction using the level set method. In *Variational and Level Set Methods in Computer Vision, 2001. Proceedings. IEEE Workshop on*, pages 194–201. IEEE, 2001.